Dislocation Density-Based Constitutive Model for the Mechanical Behavior of Irradiated Cu

A. Arsenlis, B.D. Wirth, M. Rhee

April 10, 2003

U.S. Department of Energy

Lawrence
Livermore
National
Laboratory

DISCLAIMER

This document was prepared as an account of work sponsored by an agency of the United States Government. Neither the United States Government nor the University of California nor any of their employees, makes any warranty, express or implied, or assumes any legal liability or responsibility for the accuracy, completeness, or usefulness of any information, apparatus, product, or process disclosed, or represents that its use would not infringe privately owned rights. Reference herein to any specific commercial product, process, or service by trade name, trademark, manufacturer, or otherwise, does not necessarily constitute or imply its endorsement, recommendation, or favoring by the United States Government or the University of California. The views and opinions of authors expressed herein do not necessarily state or reflect those of the United States Government or the University of California, and shall not be used for advertising or product endorsement purposes.

This is a preprint of a paper intended for publication in a journal or proceedings. Since changes may be made before publication, this preprint is made available with the understanding that it will not be cited or reproduced without the permission of the author.

This report has been reproduced directly from the best available copy.

Available electronically at http://www.doc.gov/bridge

Available for a processing fee to U.S. Department of Energy
And its contractors in paper from
U.S. Department of Energy
Office of Scientific and Technical Information
P.O. Box 62
Oak Ridge, TN 37831-0062
Telephone: (865) 576-8401
Facsimile: (865) 576-5728
E-mail: reports@adonis.osti.gov

Available for the sale to the public from
U.S. Department of Commerce
National Technical Information Service
5285 Port Royal Road
Springfield, VA 22161
Telephone: (800) 553-6847
Facsimile: (703) 605-6900
E-mail: orders@ntis.fedworld.gov
Online ordering: http://www.ntis.gov/ordering.htm

OR

Lawrence Livermore National Laboratory
Technical Information Department's Digital Library
http://www.llnl.gov/tid/Library.html

Dislocation density-based constitutive model for the mechanical behavior of irradiated

Cu

A. Arsenlis[1,*], B.D. Wirth[2] and M. Rhee[1]

[1] Lawrence Livermore National Laboratory, Livermore, CA 94551

[2] University of California, Berkeley, Berkeley, CA 94720

ABSTRACT

Performance degradation of structural steels in nuclear environments results from the development of a high number density of nanometer scale defects. The defects observed in copper-based alloys are composed of vacancy clusters in the form of stacking fault tetrahedra and/or prismatic dislocation loops, which impede dislocation glide and are evidenced in macroscopic uniaxial stress-strain curves as increased yield strengths, decreased total strain to failure, decreased work hardening and the appearance of a distinct upper yield point above a critical defect concentration (neutron dose). In this paper, we describe the development of an internal state variable model for the mechanical behavior of materials subject to these environments. This model has been developed within an information-passing multiscale materials modeling framework, in which molecular dynamics simulations of dislocation – radiation defect interactions, inform the final coarse-grained continuum model. The plasticity model includes mechanisms for

* Corresponding author, Athanasios Arsenlis, Materials Science and Technology Division Lawrence Livermore National Laboratory, P.O. Box 808, L-371, Livermore, CA 94551-0808, arsenlis@llnl.gov Ph: (925) 424-2584 FAX: (925) 424-5205

dislocation density growth and multiplication and for radiation defect density evolution with dislocation interaction. The general behavior of the constitutive (single material point) model shows that as the defect density increases, the initial yield point increases and the initial strain hardening decreases. The final coarse-grained model is implemented into a finite element framework and used to simulate the behavior of tensile specimens with varying levels of irradiation induced material damage. The simulation results compare favorably with the experimentally observed mechanical properties of irradiated materials in terms of their increased strength, decreased hardening, and decreased ductility with increasing irradiation dose.

1. Introduction

Performance degradation of structural steels in nuclear environments may limit the extended operation of current generation light-water nuclear reactors and restrict the design of advanced fission and fusion reactors (Roberts 1981, Bloom 1998, Zinkle and Ghoniem 2000, Murty 2001, Odette and Lucas 2001). While the qualitative features of microstructural evolution and mechanical property changes during neutron or high-energy particle irradiation are well established in copper alloys (Seeger 1958, Blewitt et al 1960, Greenfield and Wilsdorf 1961, Makin and Sharp 1965, Sharp 1967, Howe 1974, Sharp 1974, Muncie et al 1985, Johnson and Hirsch 1981, English et al 1987, Satoh et al 1988, Dai et al 1994, Singh et al 1995, Zinkle and Snead 1995, Singh et al 1997,

Rowcliffe et al 1998, Jenkins et al 1999, Zinkle and Singh 2000, Daulton et al 2000, Victoria et al 2000, Singh et al 2001) and are generic to most metals, quantitative and predictive models of constitutive property changes, as well as a complete fundamental understanding of the underlying microstructure – property relationships, are lacking. In this paper, we describe the first steps in the development of a physically-based plasticity model, established within a multiscale materials modeling framework, that accurately reproduces the observed stress-strain behavior of irradiated copper tested in uniaxial tension.

Irradiation at low to intermediate temperatures ($T <\sim 0.5T_m$) leads to an increase in yield and ultimate strength, a decrease in ductility (strain to fracture), a decrease in the work hardening rate, and at higher irradiation levels, the appearance of a well-defined yield point and subsequent yield drop (Seeger 1958, Blewitt 1960, Sharp 1967, Sharp 1974, Howe 1974, Dai et al 1994, Singh et al 1995, Singh et al 1997, Rowcliffe et al 1998, Victoria et al 2000, Singh et al 2001). These observations are common in a wide range of materials; but in this paper, we will focus our attention on Cu, as a representative model face centered cubic (fcc) system with relatively low stacking fault energy. It is now well established that this degradation of mechanical properties is the result of microstructural changes (Seeger 1958, Blewitt 1960, Makin and Sharp 1965, Sharp 1967, Sharp 1974, Howe 1974, Dai et al 1994, Singh et al 1995, Singh et al 1997, Rowcliffe et al 1998, Victoria et al 2000, Singh et al 2001).

The microstructure of Cu following neutron or high-energy particle irradiation has been extensively characterized by transmission electron microscopy (Muncie et al 1985, Johnson and Hirsch 1981, English et al 1987, Satoh et al 1988, Singh et al. 1995, Zinkle

and Snead 1995, Jenkins et al 1999, Zinkle and Singh 2000, Daulton et al 2000, Victoria et al 2000, Singh et al 2001) and generally consists of a high number density of nanometer-sized defects. While the number density of specific types of defects observed in fcc metals depends on the properties and composition of a particular alloy system, the observed defects in copper are general to a wide range of fcc metals and alloys, as reviewed separately by Lucas and Maziasz et al for the case of austenitic stainless steels (Lucas 1993, Maziasz 1993). In Cu, the dominant radiation produced defects are stacking fault tetrahedra (SFT), which are observed along with a lower number density of partially dissociated Frank loops (alternately called overlapping, truncated stacking fault tetrahedra, Wirth et al 2000), Frank and perfect dislocation loops, and a mixture of bubbles and voids that evolve at higher doses (Muncie et al 1985, Johnson and Hirsch 1981, English et al 1987, Satoh et al 1988, Singh et al. 1995, Zinkle and Snead 1995, Jenkins et al 1999, Zinkle and Singh 2000, Daulton et al 2000, Victoria et al 2000, Singh et al 2001). In austenitic stainless steels, the mix between Frank loops and SFT is often reversed, depending on alloy composition; and in some steels, various carbide, phosphide, nitride, and silicide precipitates may form during irradiation (Lucas 1993, Maziasz 1993). In copper, the SFT number density increases linearly with increasing dose until reaching a saturation density of $\sim 10^{24}$ m^{-3} (Singh et al 1997, Zinkle and Singh 2000). Over a wide temperature range, the mean SFT size observed in TEM studies is roughly constant at about 2.5 nm (Zinkle and Snead 1995, Zinkle and Singh 2000). The observed defect distributions are largely homogeneous in as-irradiated microstructures (Zinkle and Snead 1995, Zinkle and Singh 2000, Victoria et al 2000). However, small prismatic dislocation loops have been observed to decorate grown-in matrix dislocations

in irradiated copper above temperatures of about 200°C (Satoh et al 1988), leading to the formation of dislocation rafts and an increased network dislocation density at higher dose (English et al 1987, Singh et al 1995).

The uniaxial tensile behavior following neutron or high-energy proton irradiation is shown in Figure 1 for single crystal and polycrystalline copper, and for 316L austenitic stainless steels (Victoria et al 2000, Singh et al 2001 and Rowcliffe et al 1998). The single crystal copper specimens (Fig. 1a) were irradiated with high-energy (600 MeV) protons at 305-315 K and tested at room temperature by Dai and co-workers (Dai et al 1994, Victoria et al 2000). The polycrystalline copper specimens (Fig. 1b) were neutron irradiated at 100°C in the DR-3 reactor at Riso and tested at 100°C by Singh and co-workers (Singh et al 2001). The stainless steel (Fig. 1c) was irradiated at temperatures between 60 and 400°C by Rowcliffe and co-workers (Rowcliffe et al 1998). The resolved shear strength increases from about 10 to 105 MPa in the single crystal copper (Fig. 1a) with increasing dose, as the total shear strain to failure decreases from 1.4 to 0.55. Notably, a distinct yield point, along with a Luders-like plateau region develops for doses above 6×10^{-3} dpa [Dai et al 1994, Victoria et al 2000]. The yield strength of the OFHC polycrystalline copper increases (Fig. 1b) from about 25 to 275 MPa, while the strain to failure decreases from about 65% to 20%, with a distinct yield point observed for doses above 0.1 dpa (Singh et al 2001). The 316 stainless steel (Fig. 1c) was irradiated to approximately 7 dpa at temperatures ranging from 60 to 400°C (Rowcliffe et al 1998). At temperatures less than 400°C, distinct yield points are observed with yield strength increases in the range of 450 to 600 MPa. The steel specimen irradiated at 400°C does not exhibit a yield point, although a yield strength increase of ~350 MPa is

observed. Again, in all cases, the yield strength increases with increasing radiation dose, while the total strain to failure and the work hardening rate decrease. Above a critical dose, a distinct yield point is observed in each material followed by a subsequent yield drop. It is also important to note that in nearly every example in Figure 1, the flow stress at a given strain level is higher (offset) in the irradiated than in the unirradiated specimens.

[Insert Fig. 1 about here].

TEM examination of the post-deformation microstructures in metals irradiated beyond a critical dose frequently reveals the existence of localized deformation in the form of "defect-free channels." The channels, which appear free of irradiation induced defects, are generally on the order of 100 nm wide with a spacing of approximately 1 micron (Greenfield and Wilsdorf 1961, Brimhall and Mastel 1966, Sharp 1967, Sharp 1974, Howe 1974, Johnson and Hirsch 1980, Victoria et al 2000, Singh et al 2001, Zinkle 2002, private communication). First observed by Greenfield and Wilsdorf (1961), the appearance of channels and coarse slip steps at these length scales is now well established for a wide range of irradiated materials above a critical dose or defect density (Zinkle 2002, private communication). While a number of models have been proposed to describe the dislocation-defect interactions responsible for the removal of the irradiation defects within the channels and the sequence of events leading to channel formation; neither the dislocation - defect interactions, the channel evolution, nor the correlation between the channels and the observed tensile stress-strain behavior are well understood.

The mechanical behavior of irradiated metals is regularly correlated to the observed microstructures using either a dispersed barrier hardening model (Seeger 1958, Odette and Frey 1979, Lucas 1993, Singh et al 1997) or the cascade induced source hardening model (Blewitt 1960, Singh et al 1997). While both models predict some of the observed mechanical behavior, neither model is entirely consistent with experiments, nor describes the entire stress-strain (constitutive) behavior (Singh et al 1997, Robach et al 2003).

The dispersed barrier hardening model is typically applied to correlate changes yield strength increases to the irradiation induced defect density of metals, assuming that the contributions of individual defects to the yield strength superimpose as a root sum square (Odette and Frey 1979, Kojima et al 1991, Lucas 1993). Based on the Orowan model for the strength associated with a dispersed array of impenetrable obstacles, where the length between obstacles (pinning points), L, is given by $L \sim 1/\sqrt{Nd}$, the dispersed barrier hardening model is modified to account for the weaker radiation obstacles based on an empirical hardening coefficient, α', as:

$$\Delta\tau_{obs} = \frac{\alpha\mu b}{L}\cos(\theta/2) = \alpha'\mu b\sqrt{Nd} \qquad (1)$$

The model has been applied to a wide range of materials and irradiation conditions, and the empirical observations suggest that $\alpha' \sim 0.3$ for dislocation loops, ~ 1 for voids and ~ 0.2 for SFT (Odette and Frey 1979, Kojima et al 1991, Lucas 1993). However, as pointed out by Singh and co-workers (1997), the model is generally only applied to predict or more appropriately, to correlate microstructural observations to yield strength

increases and is believed to be unable to account for any of the post-yield deformation behavior, including the yield drop observed above a critical radiation dose.

A cascade-induced source hardening model has been proposed by Singh and co-workers (1997), based on the initial description by Blewitt (1960). The model is based on the idea that the experimentally observed yield drop results from the unlocking of grown-in matrix dislocations decorated by self-interstitial dislocation loops. These matrix dislocations serve as Frank-Read dislocation sources and, consequently, as the initiation sites of the defect free channels. As discussed in Robach et al. (2003), the model does not provide a good description for a number of irradiated alloys, including ion-irradiated copper, that exhibit a post-yield drop in strength without any observed dislocation decoration. Further, the cascade-induced source hardening model does not adequately describe the dose dependence of hardening (Singh et al 1997) and is incapable of describing the post-yield constitutive behavior following the yield drop.

In this paper, we describe the development of a dislocation density-based constitutive model for the mechanical behavior of irradiated fcc metals, established within a multi-scale materials modeling framework that incorporates information from molecular dynamics simulations of dislocation – irradiation-induced defect interactions. Section 2 describes the constitutive model in detail. In Section 3, the model predictions of the constitutive stress-strain behavior are demonstrated for single material points at the representative volume element level, and the model is used to simulate the behavior of the tensile specimens with different initial irradiation-induced defect densities. Section 4 discusses the significance of the results within the context of the mechanical properties of

irradiated metals and plastic flow localization, and Section 5 presents the conclusions and outstanding issues.

2. Constitutive Model Description

This isotropic constitutive model for irradiated metals is based on the Dispersed Barrier Hardening (DBH) models that have been previously applied to correlate the change in the yield strength of irradiated metals (Seeger 1958, Odette and Frey 1979, Kojima et al 1991, Lucas 1993) and from concepts in dislocation density-based crystal plasticity models that have been used to capture the behavior of unirradiated fcc crystals (Cuitino et al 1992, Arsenlis and Parks 2002). The resulting isotropic plasticity model assumes that the irradiation-induced defects act as shearable obstacles to mobile dislocation segments in the same manner as forest dislocation density. The effective obstacle strength of the irradiation-induced defects is assumed to depend on their size only, and the total volume fraction of irradiation-induced defects is assumed to remain constant during the course of plastic deformation. The plastic behavior of the irradiated metal is determined by the evolution of a set of internal state variables for the total dislocation density, the average dislocation line segment length, the total number density of irradiation-induced defects, and the average irradiation-induced defect size as well as the current stress state.

2.1 Finite Deformation Kinematics

The isotropic model employs the large deformation kinematics common in plasticity formulations in which the total deformation gradient, $\mathbf{F}$, is multiplicatively decomposed into an elastic, $\mathbf{F}^e$, and plastic part, $\mathbf{F}^p$, with

$$\mathbf{F} = \mathbf{F}^e \mathbf{F}^p \ . \tag{2}$$

The plastic deformation gradient evolves according to the flow rule

$$\dot{\mathbf{F}}^p = \mathbf{L}^p \mathbf{F}^p \ , \tag{3}$$

where $\mathbf{L}^p$ is the tensorial plastic flow rate. The Cauchy stress, $\mathbf{T}$, can be related to a second Piola-Kirchhoff stress, $\overline{\mathbf{T}}$, with respect to an intermediate, plastically-deformed and elastically-relaxed, configuration such that

$$\overline{\mathbf{T}} = \det\!\left(\mathbf{F}^e\right)\mathbf{F}^{e\text{-}1}\mathbf{T}\mathbf{F}^{e\text{-}T} \ . \tag{4}$$

An elastic strain measure, $\mathbf{E}^e$, corresponding to the Cauchy-Green strain tensor with the respect to the intermediate configuration is defined as

$$\mathbf{E}^e = \tfrac{1}{2}\left(\mathbf{F}^{eT}\mathbf{F}^e - \mathbf{I}_2\right) \tag{5}$$

where $\mathbf{I}_2$ is the second order identity tensor. The elastic strain and stress measures in the intermediate configuration are constitutively coupled through the fourth order elasticity tensor, $\mathcal{L}$, by the expression

$$\overline{\mathbf{T}} = \mathcal{L}\left[\mathbf{E}^e\right] \qquad (6)$$

2.2   Internal State Variable and Plastic Evolution

The focus of the continuum model is to capture the effects of radiation damage on the mechanical behavior of polycrystalline metals. For simplicity, we will ignore the effects of crystalline texture and material anisotropy and will concentrate our efforts on the plastic behavioral changes observed with varying degrees of irradiation damage. The isotropy assumption enables the general three-dimensional problem to be simplified into a one-dimensional model in terms of effective stress and strain quantities. The effective stress measure, $\overline{\sigma}$, is defined as

$$\overline{\sigma} = \sqrt{\tfrac{3}{2}\left[\overline{\mathbf{T}} - \tfrac{1}{3}tr\left(\overline{\mathbf{T}}\right)\right] : \left[\overline{\mathbf{T}} - \tfrac{1}{3}tr\left(\overline{\mathbf{T}}\right)\right]} , \qquad (7)$$

and is equivalent to the Von Mises stress in an intermediate, plastically-deformed and elastically-relaxed, material configuration. Likewise, an effective plastic strain rate, $\dot{\overline{\varepsilon}}^p$, along with the normality flow condition are introduced to simplify the constitutive definition of the tensorial plastic flow rate through the expression

$$\mathbf{L}^{\mathrm{p}} = \sqrt{\tfrac{3}{2}} \dot{\bar{\varepsilon}}^{\mathrm{p}} \mathbf{N}^{\mathrm{p}} \qquad\qquad (8)$$

where $\mathbf{N}^{\mathrm{p}}$ is the direction of plastic flow defined to be

$$\mathbf{N}^{\mathrm{p}} = \sqrt{\frac{3}{2}} \frac{\mathbf{T} - \tfrac{1}{3} tr(\mathbf{T})}{\bar{\sigma}} \, . \qquad\qquad (9)$$

With these considerations, the general three-dimensional model is simplified into a lower dimensional theory governed by the effective quantities: $\bar{\sigma}$ and $\dot{\bar{\varepsilon}}^{\mathrm{p}}$.

Since we are concerned with the behavior of polycrystalline metals at low homologous temperatures at which dislocation glide is the dominant mechanism of plastic deformation and the strain hardening (or softening) is controlled by the interactions of an evolving microstructure with the glissile dislocation density, a dislocation density-based state variable model will be implemented. The complex and evolving dislocation structure will be represented by a scalar dislocation density measure, ρ_d , with units of length per unit volume and an average dislocation line length, $\bar{l}_d$. No distinction will be made between mobile and immobile density, likewise no distinction will be made between the forest dislocation density and the glissile dislocation density. The scalar dislocation density and its average line length will evolve according to scaling laws based on more refined evolution equations developed for single crystals (Arsenlis and Tang, 2003). The description of the dislocation density state could be made more complex to allow for differentiation between an immobile forest dislocation density and a

mobile density responsible for the plastic deformation; however, such a distinction would significantly complicate the material model without substantially affecting the resultant stress-strain response.

As previously discussed, the microstructural changes that occur in fcc crystals subject to different irradiation conditions include the introduction of stacking fault tetrahedra, prismatic dislocation loops, nano-clusters of vacancies and interstitials, etc. Densities of the different irradiation-induced defects cannot be easily measured and are often not reported in the literature; therefore, for modeling purposes, it will be assumed that the densities of all of the various irradiation-induced defects increase proportionally to one another and that a single defect density will be sufficient to capture the magnitude of the total density. The irradiation-induced defect density most often reported in experimental studies of irradiated micrsotructures in copper is the number density of staking fault tetrahedra per unit volume, N_{sft}, along with their average size, d_{sft}. The irradiation-induced defects, represented though the SFT density, will be treated as shearable obstacles that impede dislocation motion and evolve during plastic deformation through a dislocation cutting mechanism. This assumption is based on the results of molecular dynamics simulations of edge dislocation interaction with perfect SFT in Cu (Wirth et al 2002). The evolution and interaction of the two defect densities, dislocation and SFT, is sufficient to reproduce the observed stress-strain behavior in a model setting.

In dislocation density-based crystal plasticity models, Orowan's relation is used to relate the glide of dislocation densities across different slip planes to the tensorial plastic flow rate. The description of the dislocation density state is much more coarse in this model; however, the tensorial plastic flow rate should scale in the same manner as the

more refined formulations leading to the following expression for the effective plastic strain rate:

$$\dot{\bar{\varepsilon}}^{\mathrm{p}} = \rho_d b \bar{v}_d \ , \tag{10}$$

where b is the magnitude of the Burgers vector, and $\bar{v}_d$ is the average dislocation glide velocity. As dislocation lines glide, their length must increase to maintain the continuity of the dislocation line resulting in an increased dislocation density. Density recovery through the statistical process of pair-wise annihilation occurs in tandem with the growth leading to the expression

$$\dot{\rho}_d = \left(\frac{2}{b \bar{l}_d} - \rho_d \frac{R_c}{2b} \right) \dot{\bar{\varepsilon}}^{\mathrm{p}} \ , \tag{11}$$

for the dislocation density evolution, where R_c is the critical capture radius of annihilation. As the dislocation density evolves, the average line length of the density evolves simultaneously. The average dislocation segment length may grow by the elongation of pre-existing segments in the volume, keeping the number density of segments in the volume constant, and it may decrease with the injection of nascent dislocation lines from Frank-Read sources, grain boundaries, incoherent defect interfaces, and other material defects. An evolution expression for the average dislocation line segment length that takes these two competing mechanisms into account is given by

$$\dot{\bar{l}}_d = \left(\frac{\bar{l}_d}{\rho_d} - \delta \bar{l}_d^3 \right) \dot{\rho}_d \ , \tag{12}$$

where δ is the dislocation line multiplication constant.

The formation of "defect-free" channels observed in *in-situ* TEM straining experiments suggests that the glide of dislocations also affects the irradiation-induced defect microstructure. Robach et al. (2003) have shown that successive passes of dislocation lines in a region may cause the region to appear free of irradiation-induced defects. They have also shown that a single dislocation passing across a defect does not necessarily result in defect absorption, but often the defect remains and acts as a pinning obstacle for the next dislocation that enters the region. Only after multiple dislocation passes may the irradiation-induced defect be absorbed.

Complete absorption of the defects is hard to confirm. The constant offset in the stress-strain response at large strains of irradiated copper single crystals compared to unirradiated behavior, shown in Figure 1 (Rowcliffe et al 1998, Victoria et al 2000, Singh et al 2001) suggests that the irradiation induced defects may not be absorbed by the gliding dislocations. Molecular dynamics simulations have shown that the irradiation-induced defects are shearable obstacles (Wirth et al 2002). It is possible that the "defect-free" channels contain residual irradiation-induced defects whose size is below the resolution of the TEM; therefore, the only evolution of the irradiation-induced defect density included in this model is the effect of dislocation cutting. As dislocations pass through a field of these obstacles, the defects are sheared by one Burgers vector for each dislocation passage. Following the interaction with enough gliding dislocations, the

original defect is sheared into two smaller defects. The rate of defect multiplication by this mechanism becomes

$$\dot{N}_{sft} = \tfrac{3}{2} N_{sft} \dot{\bar{\varepsilon}}^{\mathrm{p}} \ . \qquad (13)$$

The assumption in this analysis that the defects only evolve through dislocation cutting requires that the volume fraction of irradiation-induced defects remain constant; therefore, the average size of the irradiation-induced defects must evolve according to the expression

$$\dot{d}_{sft} = -\tfrac{1}{2} d_{sft} \dot{\bar{\varepsilon}}^{\mathrm{p}} \ . \qquad (14)$$

To close the set of equations of the model, a constitutive function for the average velocity of the dislocation density must be specified. The function must depend on the current stress and the current material state, as represented by the selection of internal state variables in the model. There is a substantial literature on both experimental and theoretical investigations of the mobility of dislocations as a function of stress, temperature, and microstructural state (Johnston and Gilman 1959, Kocks et al 1975). The resultant constitutive forms from these various sources vary widely depending on the material and deformation conditions. For simplicity, we will use a power law relationship of the form

$$\bar{v}_d = v_o \left(\frac{\bar{\sigma}}{\mu b \sqrt{\alpha \rho_d + \beta N_{sft} d_{sft}}} \right)^{1/m}, \qquad (15)$$

where v_o is a reference dislocation velocity, μ is the shear modulus, α is the dislocation forest obstacle strength, β is the irradiation-induced defect obstacle strength, and m is the strain rate sensitivity of the material. In this constitutive function for the dislocation velocity, the material strength is composed only of dislocation density forest resistance and the irradiation-induced defect resistance, with both of these acting as pinning obstacles that must be cut by gliding dislocations. Since the mechanism of resistance of the dislocation forest and the irradiation-induced defects is the same, their obstacle densities are linearly combined instead of linearly superposing their resistances.

The dislocation forest obstacle strength, α, has been shown to be a function of the type of dislocation junction that is formed between gliding dislocation line and the forest dislocation line (Wickham et al 1999). Since a single scalar density is used to represent the generally complex dislocation density state, α will have a single constant value. The irradiation-induced defect strength, β, is a function of the size of the defect. The exact functional form is unknown, but certain properties of the function are known. The strength of the defects must monotonically increase with their size. It reaches a maximum value of unity for large defects, and as the defect size approaches zero, β reaches its minimum value of zero. One such function that has these properties is the following

$$\beta = 1 - \exp\left[-\left(\frac{d_{sft}}{d_{ref}}\right)^n\right], \tag{16}$$

where d_{ref} is a reference defect size, and n is the strength sensitivity to the irradiation-induced defect size. We further constrained the reference defect size and size strength sensitivity, such that the defect strength, $\alpha' = \sqrt{\beta}$, was 0.67 for an SFT size of 2.5 nm. This value, although much higher than typically estimated from dispersed barrier hardening model correlations, was calculated from the critical bowing angle obtained from the MD simulations of Wirth et al. (2002).

The material model is intended to be employed at quasi-static strain rates and under isothermal conditions for FCC metals whose strength is derived from dislocation and irradiation damage interactions only. The model could be augmented to include other material strengthening mechanisms that work in parallel with the two mechanisms specifically included here, but including the other mechanisms at this point could obscure the influence of the irradiation-induced defects on the mechanical response of the system. As it stands, the model introduces a total of ten material-specific constants that need to be specified, and five internal state variables. Eight of the constants are used to obtain the general stress-strain behavior of the unirradiated metal, and two of them are used to specify the changes in the plastic behavior of the metal after irradiation.

3.   Model Behavior and Simulation Results

The behavior of the model will be compared to the experimental observations of Singh et al. (2001) on OFHC copper. The material parameters of the constitutive model are determined from the unirradiated stress-strain behavior shown by Singh et al. (2001) and from previous studies conducted on this material. The irradiation damage-dependent material constants will be approximated from the initial yield strength of the irradiated stress-strain response. The values of the material specific constants used to approximate the behavior of irradiated OFHC copper are provided in Table 1.

[Insert Table 1 about here]

Two series of simple tension simulations were conducted. Single material point simulations were performed to show the non-linearity in the material behavior without introducing geometric inhomogeneities. Subsequently, a series of full, three dimensional finite element simulations was performed for the sample geometry reported by Singh et al., to reveal the overall mechanical behavior observed in tension experiments. In both series of simulations, the initial density of irradiation-induced defects, N_{sft}, was varied while all other internal state variables were kept constant; revealing the effects of radiation damage on the macroscopic behavior. The simulations were conducted at a simulated total strain rate of $\dot{\varepsilon} = 3 \times 10^{-4}$ s^{-1} for five different initial irradiation-induced defect densities.

The stress-strain results of a single material point are shown in Figure 2 for five different initial irradiation-induced defect densities, varying from 4x10^{20} to 4x10^{23} m^{-3}, and a common initial SFT size of 2.5 nm. The general behavior of the constitutive model

shows that as N_{sft} increases the initial yield point increases and the initial strain

hardening decreases. In fact, at the highest irradiation-induced defect density simulated

in this work, the constitutive model strain softens after an initial upper yield point is

reached. At larger strains, the constitutive model strain hardens again, and the hardening

slope is similar to the strain hardening of the unirradiated material behavior. Also at

larger strains, the strength of the irradiated material remains larger than that of the

unirradiated material at the same level of total strain.

[Insert Figure 2 about here]

The material strain hardening/softening characteristics of the model can be

analyzed through a closed form expression. If the material is assumed to behave

homogeneously, then the effective plastic strain rate remains roughly constant after the

material has begun to plastically deform. Analysis of that condition yields the following

expression for the material point strain hardening/softening characteristics:

$$\frac{d\overline{\sigma}}{d\overline{\varepsilon}^{\,p}} = \left\{ \left[\frac{\alpha}{2(\alpha\rho_d + \beta N_{sft} d_{sft})} - \frac{m}{\rho_d} \right] \left(\frac{2}{b\overline{l}_d} - \rho_d \frac{R_c}{2b} \right) + \frac{N_{sft} d_{sft}[2\beta + n(1-\beta)\ln|1-\beta|]}{4(\alpha\rho_d + \beta N_{sft} d_{sft})} \right\} \overline{\sigma} \quad (17)$$

The unirradiated material is guaranteed to strain harden if the strain rate sensitivity is less

than 0.5. In this work, a strain rate sensitivity of $m = 5.78 \times 10^{-3}$ was used. Thus, within

this model, irradiated material can exhibit strain softening as a result of two possible

mechanisms. The first softening mechanism is accomplished through an avalanche of the

mobile density, and the second is accomplished through a reduction in the resistance of the irradiation-induced density field.

As the irradiation-induced defect density increases, the majority of the material strength is derived from forest interactions between the gliding dislocation density and the irradiation-induced defects. As the dislocation density increases, both the mobile density and forest dislocation density increase. For highly irradiated materials, the evolving forest dislocation density doesn't reduce the dislocation mobility significantly; however, the multiplication of the mobile dislocations enables each gliding dislocation to move across an increasing smaller area per unit time and encounter fewer forest obstacles. The stress required to move the dislocations at these lower velocities may increase or decrease depending on the strain rate sensitivity of the material and the influence of the dislocation forest on the overall flow strength. The strain hardening decreases monotonically with increasing irradiation-induced defect density, and above a critical value of

$$N_{sft} > \frac{(1-2m)\alpha\rho_d}{2m\beta d_{sft}} \; , \tag{18}$$

the constitutive model predicts strain softening by this mechanism. At larger strains, the dislocation density increases such that N_{sft} is below the critical value, and hardening is observed.

The second softening mechanism is strongly dependent on the strength sensitivity, n, to the irradiation-induced defect size. Since the current model assumes that the

irradiation-induced defects are not absorbed and eliminated by the gliding dislocations, but are only cut by the gliding density, the change in the resistance of the irradiation-induced defect field depends strongly on the pinning strength of the defects as a function of their size. The defect cutting increases the density of the defects while decreasing their size. For $n \leq 2$, the overall effect of obstacle cutting will be to increase the total resistance due to the irradiation-induced defect field. A value of $n = 3$ was used in these simulations; therefore, the evolution of the irradiation-induced defect density acts to further decrease the strain hardening of the constitutive model for an increase in N_{sft}. The softening contributed by this mechanism acts at every N_{sft} level, and it reduces the critical value of N_{sft} at which the over all stress-strain behavior exhibits strain softening and increases the strain level at which strain hardening is recovered. The modeling assumption that the irradiation-induced defects are not absorbed by the gliding dislocation lines ensures that the irradiated material strength will be greater than the unirradiated material strength at large strains. It is this softening mechanism that relates most closely to the formation of defect-free channels whereby the local dislocation activity has modified the irradiation-induced defect microstructure to reduce the material resistance to further dislocation activity.

Along with these two material softening mechanisms included in the constitutive model, tensile specimen geometries also lead to geometric softening in the engineering stress-engineering strain behavior from the reduction in cross-sectional area with deformation. The constitutive model was incorporated into a finite element program, and the full tension 3-D specimen geometry detailed by Singh et al. (2001) was meshed using

16000 bi-linear hexahedral elements with reduced integration. The stress-strain results of the simulations are shown in Figure 3.

[Insert Figure 3 about here]

The finite element simulation results of the uniaxial stress-strain response presented in Figure 3 clearly capture the experimental behavior summarized in Figure 1. With increasing SFT density, the yield stress increases, the nominal strain at the ultimate tensile strength decreases, an initial yield point forms above a critical SFT density of about 2×10^{23} m^{-3} and, for all but the lower defect densities after UTS, the stress at a given strain level is higher in the irradiated than the corresponding un-irradiated material. The quantitative agreement with the polycrystalline Cu (Fig 1b.) results of Singh et al. (2001) is quite remarkable. Although, the strain to failure is slightly different, this discrepancy could easily be explained by differences in the placement of extensometers on the gauge length of the specimen and non-uniformity of the deformation after UTS. In our finite element simulations, we have defined the strain based on the entire gauge length. Notably, Singh et al. (2001) report an SFT density of 2.4×10^{23} m^{-3} at 0.01 dpa, a density of $4.4\pm0.1\times10^{23}$ m^{-3} at doses higher than 0.1 dpa and a mean SFT size of 2.4 nm, which does not change with increasing dose. The model results at the two highest radiation defect densities of 2×10^{23} and 4×10^{23} m^{-3} nicely replicate the measured behavior at 0.01 dpa and the average stress-strain response for doses of $0.1 - 0.3$ dpa, respectively.

4.   Discussion

This model has been developed within an information passing multi-scale modeling materials framework, in which the final coarse-grained model is informed by finer length scale models. The objective of such models is to capture the dominant physical mechanisms within each length scale and pass this information to the higher length scale model until an appropriate level of coarse-graining is able to predict the macroscopic mechanical property observables with physical fidelity. In this work, we have utilized MD simulations to provide insight into dislocation − radiation defect interactions. We have utilized a continuum polycrystal plasticity model, informed by the MD simulations and TEM observations, to describe the single material point constitutive behavior with coarse-grained dislocation density and irradiation-defect density evolution equations; and we have utilized finite element method simulations, employing the single point constitutive model, to simulate the uniaxial tension stress-strain behavior of irradiated Cu.

The MD simulations (Wirth et al. 2002) revealed dislocation shearing of stacking fault tetrahedra and led to the derivation of the radiation defect evolution equations (13-14). Further, the critical bowing angle and corresponding α' value obtained from the MD simulations were used to constrain the defect strength contribution given by equation 16, along with the TEM observation of initial irradiation-produced SFT size of 2.5 nm. It is important to note that the critical bowing angle obtained from MD simulations, which are necessarily performed at high strain rates, certainly represents an upper bound of the hardness coefficient, α'. Indeed, for an SFT size of 2.5 nm, the parameters listed in Table 1 result in an $\alpha' = \sqrt{\beta} = 0.67$. While this value is higher than estimated from most

experimental studies (Kojima et al. 1991), the β parameter represents an average over all possible obstacles (Frank and perfect loops, partially dissociated SFT and smaller defects which are not visible in TEM examinations) that are represented in this model by a single radiation defect density, N_{sft}. In fact, our MD simulations (Wirth et al 2002) have revealed that dislocation interactions with partially truncated SFT (alternately labeled as overlapping, truncated SFT, Wirth et al 2000) result in defect absorption by the moving dislocation. However, in this case, absorption results in the formation of a closely spaced super-jog pair, which subsequently acts as an Orowan obstacle, and therefore exhibit an increased α', that is completely pinched off, leaving a perfect, prismatic dislocation loop in its place. Thus, the chosen value of α' represents an average over all possible radiation defects and interaction mechanisms.

Rodney and co-workers (2001) have also recently developed a dislocation evolution model, based on observations from MD simulations to describe the post-yield stress strain behavior of irradiated metals. Their model is based on MD simulations of edge dislocation – self-interstitial cluster interactions in Ni, where they observed cluster incorporation into dislocation super-jogs (Rodney et al. 2001). In those simulations, subsequent dislocation bowing and re-emission of the super-jogs as a perfect loop was not observed. And thus, the constitutive model developed by Rodney and co-workers (2001) assumes that mobile dislocations absorb all radiation defects. This model does show the formation of a distinct yield point in their single material point (constitutive model) stress-strain behavior, which qualitatively reproduces some of the experimental observations. However, the defect annihilation mechanism with complete defect destruction results in a single material point constitutive model where the irradiated

stress-strain curve rapidly softens following the yield point and returns to the unirradiated curve, with exactly the same work hardening behavior. As discussed previously, neither the magnitude of the initial yield drop nor the stress offset in irradiated materials at a fixed strain, experimentally summarized in Figure 1 (Rowcliffe et al. 1998, Victoria et al. 2000, Singh et al. 2001), support this model of complete defect absorption.

The model presented in equations 2 through 18 and Figures 2 and 3 does not contain an implicit length scale, and, further subsumes both the mobile and immobile dislocation density into a single effective dislocation density. The description of the dislocation density could be made more complex to allow for differentiation between an immobile forest dislocation density and a mobile density responsible for the plastic deformation; however, such a distinction would significantly complicate the material model without substantially modifying the stress-strain response. The lack of a length scale neither explicitly includes, nor discounts the formation of defect-free dislocation channels. Implementation of the single material point constitutive law into a large geometry change finite element simulation does reproduce the macroscopic localization and necking phenomena observed during uniaxial tensile tests.

Defect-free dislocation channel formation and localized material deformation is clearly ubiquitous in irradiated metals (Greenfield and Wilsdorf 1961, Brimhall and Mastel 1966, Sharp 1967, Sharp 1974, Howe 1974, Johnson and Hirsch 1980, Victoria et al 2000, Singh et al 2001, Zinkle 2002, private communication) and certainly has important consequences to material deformation and fracture. However, the implication of this model is that the microscopic mechanisms and length scales governing the formation of defect free dislocation channels may not be needed to predict the

macroscopic stress-strain behavior. As just mentioned, this model does not explicitly include defect free dislocation channel formation, yet is able to quantitatively reproduce the measured uniaxial stress-strain mechanical behavior. The strain hardening/softening characteristics of the model result from the combination of two mechanisms. The first softening mechanism is an avalanche of the mobile density, as in the model of Hahn for yield point phenomena of bcc metals (Hahn 1962), and the second is a reduction in the resistance of the irradiation-induced defect density field. The modeling assumption that the irradiation-induced defects are not absorbed by the gliding dislocation lines ensures that the irradiated material strength will be greater than the unirradiated material strength at large strains. It is this second softening mechanism that relates most closely to the formation of defect free channels whereby the local dislocation activity has modified the irradiation-induced defect microstructure to reduce the material resistance to further dislocation activity.

Thus, it is tempting to conclude that dislocation channels may not directly correlate to the observed yield drops. Indeed, such channels are observed in materials whether or not distinct yield point drops are measured (Victoria et al. 2000, Zinkle, private communication 2002), as well as throughout the stress-strain curve, including tests interrupted prior to yielding and those that exhibit a yield drop and a subsequent return to work hardening (Victoria et al. 2000). The plastic deformation of irradiated materials is undoubtedly occurring in material regions that show the apparent clearing of defects, which is evidence of the inhomogeneity of plastic deformation at nanometer length scales, and the defect clearing (through dislocation shearing/cutting interactions, as well as possibly from defect absorption and re-emission events) provides a tangible

picture of the inhomogeneity. However, it is important to note that the plastic deformation of unirradiated materials is an inhomogeneous process at the nanometer length scale as well, but there are no defects to delineate the deformed from the undeformed regions as in the irradiated material. In fact, comparisons of the surface slip step profiles of both irradiated and unirradiated copper single crystals suggests that the heterogeneity of the plastic deformation does not substantially change with irradiation at high strains (Greenfield and Wilsdorf 1961). Unraveling the role of defect free channels on the observed uniaxial stress-strain behavior, as well as quantifying the degree of heterogeneity of dislocation channel deformation relative to unirradiated materials will likely require a detailed study of surface slip step evolution, in-situ deformation studies and post-mortem characterization of carefully controlled interrupted uniaxial tension tests, in addition to a wide range of multi-scale materials simulation techniques.

Homogeneous isotropic constitutive models are well accepted for simulating the macroscopic stress-strain constitutive behavior of polycrystalline metals (Arsenlis and Parks 2002, Hahn 1962, Kocks 2001), even though they deform in a non-homogenous fashion. Thus, it is natural to apply such models to irradiated metals, with an extension to include the radiation-produced defect obstacle interactions, as presented in this work. In this work, we have varied the radiation defect density from 4×10^{20} to 4×10^{23} m^{-3} with an initial SFT size of 2.5 nm, based on experimental observations (Zinkle and Singh 2000) and compared the model results with experimental uniaxial stress-strain data (Singh et al. 2001) to demonstrate the fidelity of the multiscale modeling approach. In principle, the constitutive model in this work can be combined with a model for the radiation defect evolution (defect type, size and number density) as a function of irradiation and material

variables to obtain a truly predictive model for the mechanical behavior changes of irradiated materials.

Further, this constitutive model framework is general and can be applied to both more complicated fcc metals and alloys, such as austenitic stainless steels, as well as bcc alloys. The implementation of a bcc model will be the focus of future modeling efforts and will require a temperature dependent dislocation velocity law to account for the inherent lattice resistance and the material's response to strain localization and the formation of adiabatic shear bands.

5.   Conclusions

An internal state variable-based isotropic plasticity model for the uniaxial stress-strain constitutive behavior of irradiated materials has been presented. This model has been developed within an information passing multi-scale modeling materials framework, in which the final coarse-grained continuum model is informed by MD simulations of dislocation – stacking fault tetrahedra interactions. The plasticity model includes mechanisms for dislocation density growth and multiplication and for irradiation-induced defect density evolution with dislocation interaction.

The dislocation density evolution model is based on crystal plasticity models that have been used to capture the behavior of unirradiated fcc crystals and represents the complex and evolving dislocation structure through a scalar dislocation density measure, ρ_d, with units of length per unit volume and an average dislocation line segment length,

$\bar{l}_d$. The scalar dislocation density, which includes both the mobile density and immobile forest dislocation density, and its average line length evolve according to scaling laws based on more refined evolution equations developed for single crystals. Orowan's relation is used to relate the net glide of dislocation densities across different slip planes to the tensorial plastic flow rate.

The dislocation density evolution model has been augmented to account for radiation produced defects based on the Dispersed Barrier Hardening concepts, also incorporating information obtained from MD simulations. The MD simulations revealed dislocation shearing of SFT, without defect absorption, and led to the derivation of equations describing the evolution of the radiation defect population during deformation. Further, the MD results were used to constrain the strength contribution of these defects, whose size and number density in the model were representative of experimental TEM observations of SFT size and number density. A constitutive function for the average velocity of the dislocation density completed the model. In this work, we have specified the velocity relationship as a power law, whereby the dislocation density forest resistance and the irradiation-induced defect resistance act as pinning obstacles that must be cut by gliding dislocations.

The general behavior of the constitutive (single material point) model shows that as the defect density increases, the initial yield point increases and the initial strain hardening decreases. Implementation of the final coarse-grained constitutive model into a finite element framework was used to simulate the behavior of tensile specimens with varying levels of irradiation induced material damage. The simulation results compare favorably with the experimentally observed mechanical behavior of irradiated materials

in terms of predicting increased strength, decreased hardening, and decreased ductility with increasing irradiation dose.

The description of the dislocation density state could be made more complex to allow for differentiation between an immobile forest dislocation density and a mobile density responsible for the plastic deformation; however, such a distinction would significantly complicate the material model without substantially affecting the general stress-strain response that it produces. Future modeling efforts will focus on coupling the constitutive model to a microstructure evolution model to predict the mechanical property changes as a function of irradiation variables and, the development of a model for irradiated bcc alloys, which will require a temperature dependent dislocation velocity law to account for the inherent lattice resistance and the material's response to strain localization and the formation of adiabatic shear bands.

Acknowledgements

REFERENCES

Arsenlis, A., and Parks, D. M., 2002, *J. Mech. Phys. Solids*, **50**, 1979.

Arsenlis, A., and Tang, M., 2003, *Modelling Sim. Mat. Sci. Engrg.*, **11**, 265.

Blewitt, T.H., Coltman, R.R., Jamison, R.E., and Redman, J.K., 1960, *J. Nucl. Mat.,* **2**, 277.

Brimhall, J.L. and Mastel, B., 1966, *App Phys Let*, **9**, 127.

Bloom, E.E., 1998, *J. Nucl. Mat.,* **258-263**, 7.

Cuitiño, A. M., and Ortiz, M., 1992, *Modelling Sim. Mat. Sci. Engrg.*, **1**, 225.

Dai, Y., Gavillet, D., Paschoud, F., and Victoria, M., 1994, *J. Nucl. Mat.,* **212-215**, 393.

Daulton T.L., Kirk M.A., and Rehn L.E., 2000, *Phil Mag A,* **80**, 809.

English, C.A., Eyre, B.L. and Muncie, J.W., 1987, *Phil Mag A,* **56,** 453.

Greenfield, I.G., and Wilsdorf, H.G.F., 1961, *J. App. Physics*, **32,** 827.

Hahn, G.T., 1962, *Acta Met.*, **10**, 727.

Howe, L.M., 1974, *Rad Effects*, **23** 181.

Jenkins, ML, Kirk, MA, and Fukushima, H., 1999, *Journal of Electron Microscopy,* **48**, 323.

Johnson, E. and Hirsch, P.B., 1981, *Phil Mag A,* **43**, 157.

Johnston, W. G., and Gilman, J., 1959, *J. Appl. Phys.,* **30**, 129.

Kocks, U. F., Argon, A. S., and Ashby, M. F., 1975, *Prog. Mat. Sci.,* **19.**

Kocks, U.F., 2001, *Mat Sci & Eng A*, **317**, 181.

Kojima S. and Zinkle, S.J., 1991, *J. Nucl. Mat.,* **179-191**, 982.

Lucas, G.E., 1993, *J Nucl Mat*, **206,** 287.

Makin, M.J. and Sharp, J.V., 1965, *Phys. Stat. Sol.,* **9**, 109.

Makin, M.J., 1970, *Phil Mag,***21**, 815.

Maziasz, P.J., 1993, *J Nucl Mat,* **205,** 118.

Muncie, J.W., Eyre, B.L. and English, C.A., 1985, *Phil Mag A,* **52**, 309.

Murty, K.L., 2001, *JOM,* **53 no 7**, 8.

Odette, G.R. and Lucas, G.E., 2001, *JOM,* **53 no 7**, 18.

Odette, G.R. and Frey, D., 1979, *J. Nucl. Mat.,* **85-86**, 817.

Robach, J.S., Robertson, I.M., Wirth, B.D. and Arsenlis, A., 2003, *Phil Mag*, **83**, 955.

Roberts, J.T.A., 1981, *Structural Materials in Nuclear Power Systems*, (Plenum Press: New York and London).

Rodney, D., Martin, G., and Brechet, Y., 2001, *Mat Sci & Eng A*, **309-310**, 198.

Rowcliffe, A.F., Zinkle, S.J., Stubbins, J.F., Edwards, D.J., and Alexander, D.J., 1998, *J Nucl Mat,* **258-263,** 183.

Satoh, Y., Ishida, I., Yoshie, T., and Kiritani, M., *J Nucl Mat*, **155-157,** 443.

Seeger, A., 1958, *Proceedings of the 2nd U.N. International Conference on Peaceful Uses of Atomic Energy (Geneva, United Nations),* **6**, 250.

Sharp, J.V., 1967, *Phil. Mag.,* **4**, 77.

Sharp J.V., 1974, *Acta Met,* **22**, 449.

Singh, B.N., Horsewell, A., Toft, P., and Edwards, D.J., 1995, *J Nucl Mat,* **224,** 131.

Singh, B.N., Foreman, A.J.E., and Trinkaus, H., 1997, *J Nucl Mat,* **1997,** 103.

Singh, B.N., Edwards, D.J. and Toft, P., 2001, *J Nucl Mat,* **299,** 205.

Victoria M., Baluc N., Bailat C., Dai Y., Luppo M.I., Schaublin R., and Singh B.N., 2000, *J Nucl Mat*, **276,** 114.

Wickham, L. K., Schwarz, K. W., and Stölken, J. S., 1999, *Phys. Rev. Lett*., **83**, 4574.

Wirth, B.D., Bulatov, V.V., and Diaz de la Rubia, T., 2000, *J Nucl Mat*, **283-287,** 773.

Wirth, B.D., Bulatov, V.V., and Diaz de la Rubia, T., 2002, *J Eng Mat & Tech,* **124**, 329.

Zinkle, S.J. and Ghoniem, N.M., 2000, *Fusion Engineering & Design,* **51-52**, 55.

Zinkle, S.J. and Snead, L.L., 1995, *J Nucl Mat,* **225,** 123.

Zinkle, S.J. and Singh, B.N., 2000, *J Nucl Mat,* **283-287,** 306.

Table 1. Material specific constants and initial conditions for the internal state variables used to model the plastic behavior of irradiated polycrystalline OFHC copper in uniaxial tension.

Elastic Constants	$\mu = 48.5$ GPa
	$\nu = 0.300$
Burgers Vector	$b = 0.25$ nm
Dislocation Mobility	$v_o = 4 \times 10^{-6}$ m/s^{-1}
	$m = 5.78 \times 10^{-3}$
	$\alpha = 0.090$
Dislocation Evolution	$\delta = 8 \times 10^{-3}$
	$R_c = 8.5b$
Irradiation Defect Strength	$d_{ref} = 3$ nm
	$n = 3.0$
Initial Internal State	$\mathbf{F}^e = \mathbf{I}_2$
Variable Conditions	$\rho_d = 5 \times 10^{13}$ m^{-2}
	$\bar{l}_d = 1 \mu$m
	$d_{sft} = 2.5$ nm

Figure 1. Summary of measured uniaxial stress-strain behavior of irradiated metals, a) single crystal copper (Victoria et al. 2000), b) polycrystalline copper (Singh et al. 2001) and c) austentitic stainless steels (Rowcliff et al. 1998).
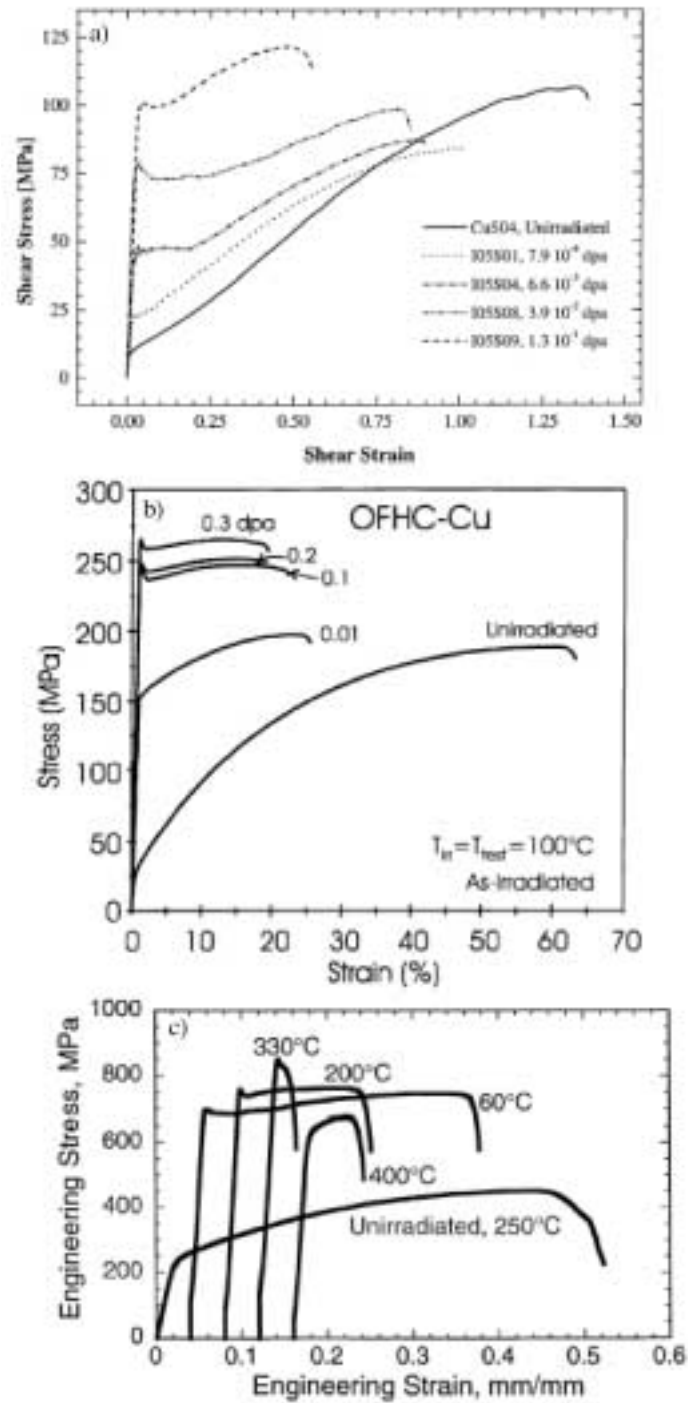
Figure 2. Simulated effective stress-effective strain behavior of a single material point of an irradiated OFHC copper polycrystal with varying densities of irradiation-induced defects.
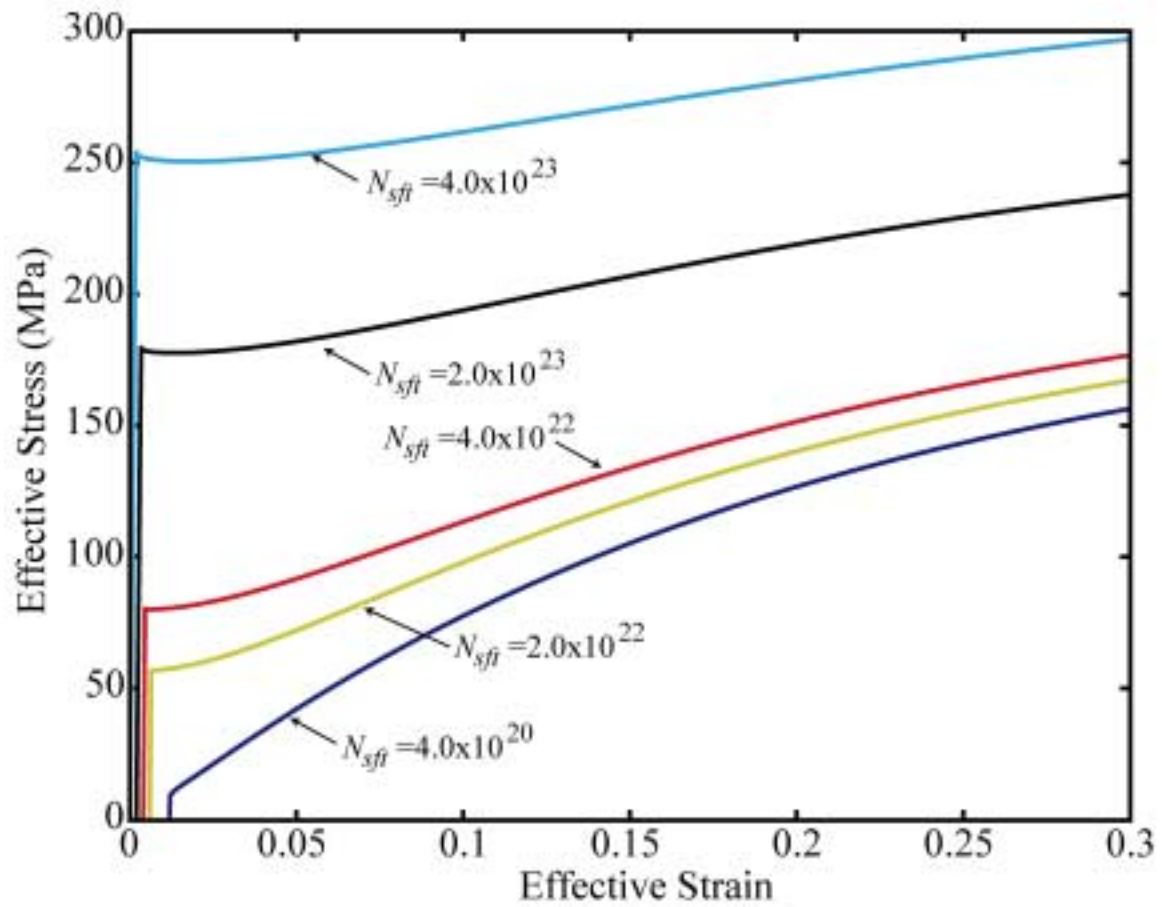
Figure 3.   Simulated engineering stress-engineering strain behavior of an irradiated OFHC copper polycrystal with a tensile specimen geometry described by Singh et al. (2001)